Wind Load Assessment of a Large Radar Antenna using Measurements and Simulation

Rohitha Weerasinghe, Thomas Bunn

University of the West of England, Bristol, UK

Abstract. Radar structures are subject to heavy wind loads due to the physical size of such structures. This paper contains the methodology and assessment of a project which set out to accomplish an improved method for modelling wind loads on a radar structure. The new method employs the use of computational fluid dynamics (CFD) to create a simulation of the conditions. Several studies on the approach to CFD testing were undertaken to optimise the process. Dimensions of domain volume and mesh density were examined for their effect on the computed solutions, as well as run time. Once an efficient set-up had been found, a scale model of the radar was analysed. Pressure distributions across the antenna face were studied from four cases, in which the prevailing wind approached from a different direction relative to the system (0°, 45°,90° and 180°). To validate the results from the CFD, a low-speed wind tunnel test was conducted. The experimental measurements were compared to the computed results and common trends were shown to exist between both sets of data.

1. Introduction

1.1 Windloading

Traditionally, radar antennas use a grated metallic structure to transmit and receive RF waves. Although these antennas can often have a large surface area, the slotted area helps to combat wind conditions. However, with the development of solid state radar, modern active electronically scanned arrays require a very different type of structure. These delicate modules are required to be protected from the environment by a housing that can protect from the elements whilst also being radio frequency (RF) transparent. This new set of requirements has led to composites engineering being a primary material in radome construction. However, because these composite architectures often form a large solid surface, they are prone to the effects of wind loading, which can cause distortion and deflection in the radar beam. For a better radar design, the effects of these loads must be properly understood and allowed for in design to ensure precision and accuracy. Because the radar to be studied in this investigation is a large ground based radar, it can be initially considered to behave as a simple building structure. The wind loading is important to understand the performance of the antenna design; especially regarding the ability to control antenna distortion and deflection in more challenging environmental conditions. BS6399-2 (BSI, 2002) outlines a code of practice for wind loads on buildings. It offers two different methods for calculating the loads on a building. The methods are distinguished by their complexity and still offer a conservative estimate on the wind loads a building may face.

The standard contains large amounts of data on key building features and accounts for factors including altitude of the site, surrounding building heights and topography.

1.2 Boundary Layer

Boundary layer separation is a phenomenon that occurs when the velocity outside the boundary layer

Content from this work may be used under the terms of the Creative Commons Attribution 3.0 licence. Any further distribution of this work must maintain attribution to the author(s) and the title of the work, journal citation and DOI.
Published under licence by IOP Publishing Ltd

decreases, consequentially increasing pressure, in accordance to Bernoulli's equation (Buresti, 2000). As this happens the deceleration causes the boundary layer velocity profile to deform to a point where flow closer to the wall actually starts to move in the opposite direction of the free stream flow. It is at this point a wake forms, where the flow conditions are unsteady and the boundary layer becomes turbulent. Buresti (2000) goes on to state that, because of the larger amount of energy in turbulent boundary layers, they stay attached to a surface for much longer and are more resistant to separation. Curved surfaces are often used to demonstrate the difference in behaviour of laminar and turbulent boundary layers because separation occurs at sharp edges regardless of type. The behaviour of a boundary layer and the wake that an object leaves are used to characterise the body type of the object. The two types of bodies are aerodynamic and bluff. Aerodynamic shapes are ones which have a thin boundary layer running across almost the complete surface length which leaves a small, steady wake. These shapes include aerofoils, which are used in aeronautics and motorsport to create aerodynamic forces such as lift or downforce by creating a pressure differential through understanding of this effect. Conversely, a bluff body is a body in which separation occurs prematurely from a surface and a much larger and unsteady wake is observed. As Buresti (2000) highlights, the flow orientation can be influential in the characterisation of a body, for instance a body may be considered aerodynamic in some flow directions and bluff in others. Examples of bluff bodies include blocks and plates but also cylinders.

Both types of bodies are subject to drag; a force acting against the movement of an object. In engineering, drag is generally an undesirable force as it can cause losses in a system. Although all bodies are impacted by this force the main reasoning behind and subsequent magnitude of the drag is different dependent on body type. For aerodynamic bodies the friction caused by the fluid moving over a surface is the primary source of drag and is known as friction drag. However, in a bluff body, the large wake, due to separation, causes a lower pressure at the rear of the body than at the front. This is known as pressure drag and is much more significant contributor to the total system drag.

For wind engineering problems, the proximity of the ground can also be an important consideration as a natural boundary layer occurs between the air and the earth's surface. The natural boundary layer can be highly variable and is dependent on topographical location and features such as mountains, lakes and other nearby buildings. For even more in depth calculations the Rossby number must be considered; which concerns itself with latitude and the earth's rotation.

It can be hard to replicate in tests and doing so often requires the use of strakes to create representative atmospheric conditions and trip strips to emulate ground roughness. Rae *et al.* (1984) state that the boundary layer profile at the proposed site, should it not be known, can be estimated per:

$$\frac{C}{C_{ref}} = \left(\frac{h}{h_{ref}}\right)^{\alpha} \qquad (1)$$

1.3 Computational Modelling

A lot of properties and characteristics about how fluids behave are well understood but can be difficult to model analytically. Computational fluid dynamics (CFD) use mathematical models to model properties and provide results. Fluid properties can be described by a solvable mathematical equation, known as the Navier-Stokes equation.

For a computer to solve this equation the problem must be discretised. This means reducing a continuous domain down to a finite number of points which the computer can solve to. The way in which this is done is by using a grid or mesh which points can be taken from. Solving the Navier-Stokes equation using a computer requires the use of vast processing power, which is often not feasible for many applications. To counter this, CFD uses turbulence models, which make assumptions and estimations to some of the terms of the equations. Whilst this reduces the accuracy of the solution, it is highly beneficial, through reducing time and cost. Often the type of turbulence solver is selected after consideration of the specific problem

Steady state Reynolds-averaged Navier-Stokes equations are used in representing the flow field. The conservation of mass is given as;

$$\frac{\partial}{\partial x_i}(\rho u_i) = 0 \qquad (2)$$

and the conservation of momentum is written as:

$$\frac{\partial}{\partial x_i}(\rho u_i u_j) = -\frac{\partial p}{\partial x_i} + \frac{\partial}{\partial x_j}\left[\mu\left(\frac{\partial u_i}{\partial x_j} + \frac{\partial u_j}{\partial x_i} - \frac{2}{3}\delta_{ij}\frac{\partial u_k}{\partial x_k}\right)\right] + \frac{\partial}{\partial x_j}(-\rho\overline{u_i' u_j'}) \qquad (3)$$

The Reynolds stress above must be modelled and it can be achieved via a Boussinesq hypothesis.

$$-\rho\overline{u_i' u_j'} = \mu_t\left(\frac{\partial u_i}{\partial x_j} + \frac{\partial u_j}{\partial x_i}\right) - \frac{2}{3}\left(\rho k + \mu_t\frac{\partial u_k}{\partial x_k}\right)\delta_{ij} \quad (4)$$

Here, is the turbulent viscosity and is the turbulent kinetic energy. A turbulence model has to be employed to close this where the *k-ε* - model has been used in this work.

2. problem definition

2.1 Meshing and Boundary Conditions

When using CFD to model wind a domain of simulation volume must be used. This is an area around the subject of the study used to limit the size of the mesh. In practice a realistic domain would require an unnecessarily large mesh and calculate data for a large number of irrelevant points, wasting computing time. The domain must be carefully chosen so the solution is unaffected by any false effects caused by the boundaries of the simulation area. One domain characteristic, in order to allow the turbulent wake and recirculation zone to fully develop, is to have a greater volume of the domain downwind of the structure (Knapp, 2007). The magnitude of the simulation volume is not the only factor that influences the size of the mesh. The mesh density is also an important factor; a finer mesh, with more elements will give a more accurate solution but will also require more computing power. To properly analyse a problem, the mesh needs to be much denser at points of interest of to the study such as boundary layers, in this case on the faces of the antenna structure. The rest of the domain is of less concern and a fine mesh density here would be counterproductive, slowing down the solution by computing irrelevant data. One method is to place the structure in a zone four times larger than itself and populate it with a finer unstructured mesh (Huang, Li and Xu, 2007). An unstructured mesh, i.e. a tetrahedral (tet) dominant mesh, is usually afforded to shapes with more complex shapes. A structured mesh is a hexahedral (hex) dominant one and can often have a lower cell count than a comparable unstructured mesh. For a mesh to be most effective it should be aligned with the flow, however, with problems which include complex flow features this is much harder to achieve. Whilst a well-constructed mesh which carefully accounts for features may ultimately result in faster computing, the time taken to construct such a mesh make this option impractical (Harris, 2013). Hexahedral meshes are often better at aligning cell faces to flow features but the comparative inflexibility to tetrahedral meshes mean they are not always preferable.

2.2 Approach to Wind Loading.

The primary reason for the interest in wind loading is to provide values from which a suitable architecture can be designed. These initial approximations are used to calculate the beam deflection of the radar system and because of the importance of this design driver, a more accurate figure is required. The current load assumes a uniform pressure and is applied to all faces of the antenna facing the wind direction. The magnitude of this pressure was given by.

$$p = \frac{C_d \rho V^2}{2} \qquad (5)$$

The drag coefficient C_d was estimated by studying lookup tables for different aspect ratio buildings and graphs of how this figure changed if the surface was not at a position normal to the wind. Furthermore, the slope front face of the radome has been factored in and the coefficients for winds in the normal direction to each side are shown below

Table 1: Drag coefficients radar faces, assuming a wind direction normal to surface

	Front	**Aft**	**Side**
Drag Coefficient	1.08	1.13	1.12

2.3 CFD Approach.

The aim of the approach study was to study the results mesh independency, domain suitability and the applicability of two different turbulence models; the Reynolds Stress Model and the k-ε model. To achieve this, a scale model of the radar was solved in Fluent for a headwind scenario. Once the optimum set up was found the radar was tested against a wind coming from three other directions; from an angle (45°), from the side (90°) and from behind (180°). The CFD results from the scale model were then compared to the current theoretical approach before being validated using a wind tunnel test. The air properties are given in Table 2.

Table 2: Fluid properties

Air Density (kg/m^3)	**Wind Speed (m/s)**	**Air Dynamic Viscosity (Pa s)**
1.2255	30	1.983e-5

The boundary conditions of the mesh area are another important control that is used to better model a turbulent flow. It is in the selection of these that aspects such as a terrain friction factor can be included. The conditions that are often chosen for the domain of the problem are designed to interfere with the solution as little as possible. When defining the domain boundaries, the edges and upper surfaces must be modelled as non-slip or symmetries (Reiter, 2008). The inlet must account for the wind speed and turbulence characteristics of the air flow. A target profile must be developed upstream of the structure before any estimates of pressure have been calculated (Clannachan *et al.*, 2009). At the outlet boundary, the static pressure is defined as zero. A velocity and turbulence profile is not used here to avoid causing an artificial fluctuation of pressure within the simulation volume (Knapp, 2007).

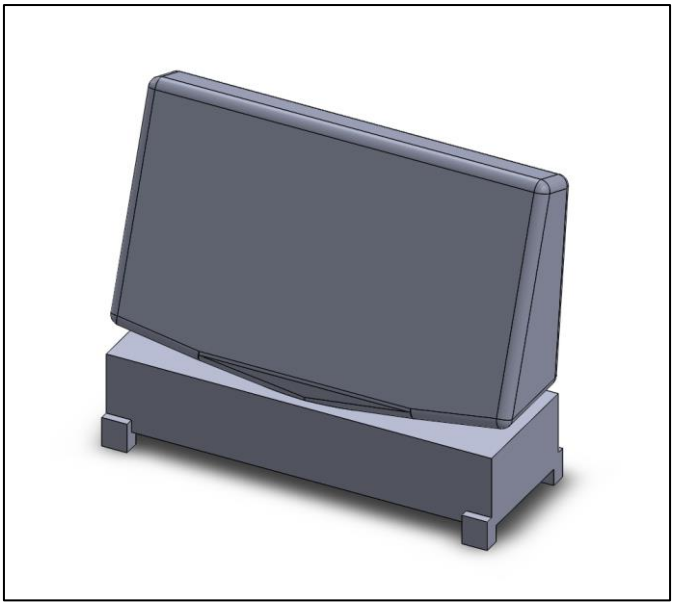

Figure 1 CAD Model of Radar Structure

A simple CAD model was created in SolidWorks2016 from dimensions provided by BAE Systems. Due to the basic nature of the model, no work was needed to simplify features of the model before importing to the Fluent CFD package. The model was built using the full-scale dimensions and then scaled inside SolidWorks software. Two different domains were modelled, the first was an accurate representation of the working section of the wind tunnel that the model would be tested against and the

second was a smaller domain based on suggestions from literature. The dimensions of the second domain were scaled using the width (L_x) of the radar (0.18m) and were five times this length in the upwind direction and either side of the structure. The domain height was designed to be four times the height of the structure (L_y). In alignment with the simulation volumes studied in literature, the downwind length was extended to account for the turbulent wake of the flow; this length was $15L_x$. Both these models were then meshed with a first estimate of a suitable mesh and analysed to gauge any discernible difference.

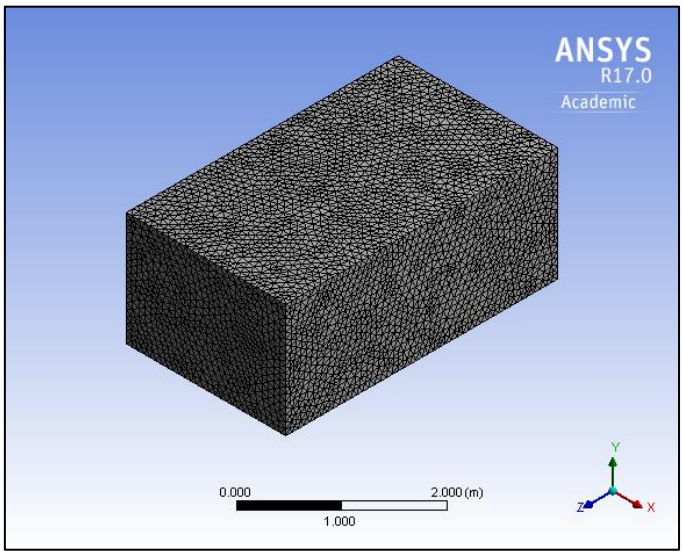

Figure 2 Domain Study: Mesh Structures for tunnel

In conclusion, the quality of results arising from the increased dimensions and additional mesh elements, was deemed insufficient to warrant the continued use of the domain which accurately represented the wind tunnel section. Following the domain study, the literature based domain was used for all CFD runs.

Further mesh dependency tests were carried out to see how sensitive the mesh fineness to the problem. Despite the higher run time, the Fine Mesh was used in calculations. The lower minimum element size allowed it to give a more accurate look at the effects of the air at the antenna, as well as having the added benefit of improving the mesh quality.

Spatial discretization schemes are required to approximate convection terms for flow equations which calculate pressure, momentum, turbulent kinetic energy and turbulent dissipation rate. Several discretization schemes are available for use. The set-up was adjusted so that momentum, turbulent kinetic energy and turbulent dissipation rate used a first order scheme whilst pressure maintained a second order one. The guide also suggests that once a better convergence appears available, second order can be switched on and the calculation continued.

3. modelling and simulation

3.1 Mathematical Modelling

The set-up was adjusted so that momentum, turbulent kinetic energy and turbulent dissipation rate used a first order scheme whilst pressure maintained a second order one. The guide also suggests that once a better convergence appears available, second order can be switched on and the calculation continued.

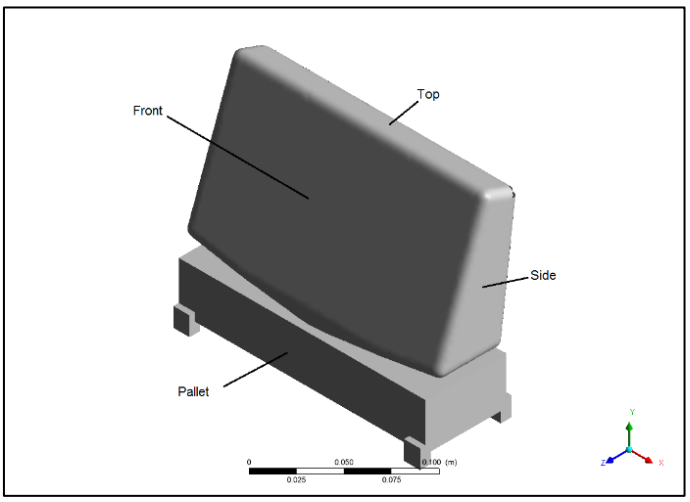

Figure 3 Named faces of radar model

Different views from the four runs were studied to identify the gradients of most interest. The resultant data was used to propose pressure tap placements for the experimental model, which would be used to validate the CFD. To avoid confusion the faces of the model have been assigned designated terms by which they are referred to regardless of wind direction; they are shown in Figure 3. The plane at which the antenna and pallet meet is hitherto referred to as the interface line.

3.2 Headwind Case

Because the headwind case had been used extensively through the suitability studies some expectation of the solution had been gained. Pressure contour plots had been generated drawing some light analysis and comment previously. Evidently, the face subjected to the highest pressures is also the one which is normal to the direction of airflow. As the wind flows around the antenna it can be seen to create areas of low pressure on the radii after which a zone of low pressure appears behind the antenna. The contour lines on the top and side face of the antenna indicate a quite uniform change drop across the sides to the rear. Unlike the front, no sizeable gradients appear on the radii at the rear of the antenna. The rear face of the antenna displays a relatively consistent pressure difference, save for one area roughly in the centre which is higher than most.

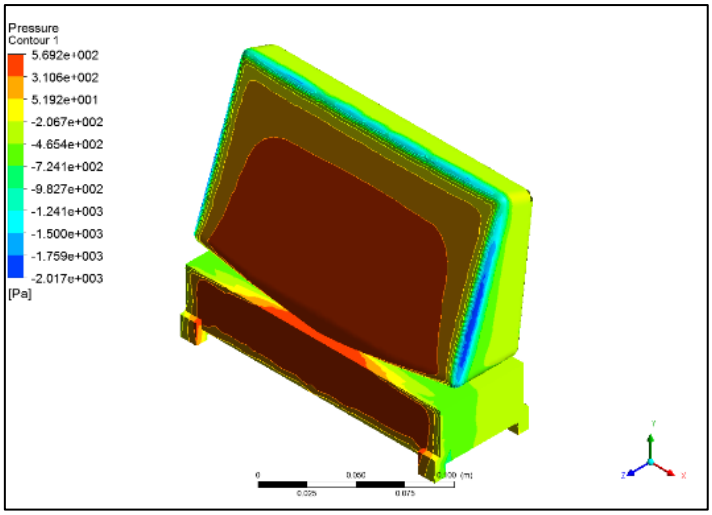

Figure 4 CFD Headwind Analysis: Pressure Contour

From this run it was deduced that taps across front surface and radii would present the most useful data, with a higher concentration of readings nearest the edges of the radar, where the changes in pressure

were most considerable. Readings from the side and top faces in line with flow direction (Z-axis in this case) were deemed worthwhile near the front radii so that a good picture of the fluctuation could be built. The variation across the flow (Y direction in this case) on these faces though, was much less and considered to be of less relevance.

This face, at a normal to the headwind contained the highest pressures seen in the system, with the maximum occurring on the pallet section. The areas of lowest pressure occurred at the radial edges of the antenna. It was readily apparent that the effect of these had some bearing on the pressure distribution as the sharp edges on the pallet below contained such an effect. To analyse these gradients, lines were added to the face of the antenna which could select a desired number of samples and be used to form a graph. Unfortunately, it was not possible to map a line around the radial of the structure, where the most extreme pressure gradients occurred. To counter this, sample lines were added to adjacent faces of the radar to build an understanding of the pressure differentials around the curved surfaces and points on the radial edges probed individually at suitable increments. Five surfaces were examined, namely the front, back, top and only one each of the side and underside faces, due to the symmetry in the YZ plane of the radar. Each of these five surfaces was fitted with a longitudinal and lateral sample line. In general, longitudinal lines are on the YZ plane or planes offset from it and display pressure as the wind moves over or under a face.

Figure 5 shows a profile of pressure drop over all faces as the flow moves around the sides of the radar. This graph shows how rapidly the pressure decreases before and during the radial edge, between 80mm and 95mm the change in pressure is 2.013KPa. Joinings or fittings located in this area would potentially be subject to extremely high forces. Furthermore, the profiles of the curves before and after the lowest pressure are markedly similar; almost a reflection of one another. After being rapidly accelerated and then decelerated, the flow regains a seemingly more constant nature on the rear face, albeit at a much lower pressure than at the front.

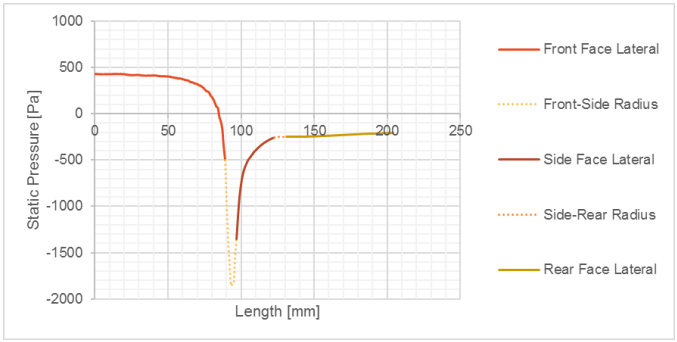

Figure 5 CFD Headwind Analysis: Lateral pressure changes across faces and radial edges

3.3 Backwind Case

As the cross-sectional area of the radar facing the wind was similar between the headwind and backwind cases, comparisons have been drawn between the two. The geometry of the structure, however, presents a markedly different obstacle for the wind to bypass.

The predominant face in the backwind case displayed a much larger area of high pressure than the headwind. Again, after the all faces not at a normal to the wind were enclosed in an area of low pressure. As the angle of the rear face of the antenna was much shallower than the front, the pressure contour behaved in a much more similar way to the square face of the pallet. The radial edges facing the flow direction were again the features with the lowest pressure reading. The top face was more exposed to the oncoming wind and a higher overall pressure may have been expected here as a result, although the plot suggested otherwise. The most sheltered surface from the free stream, this time the front face, showed a less consistent pressure profile. However, there was again a peak of pressure in the centre of the face but was much more prominent than in the headwind case.

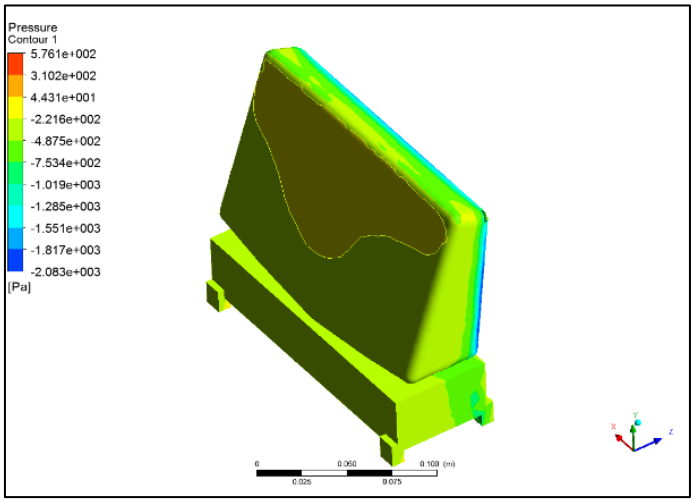

Figure 6 CFD Backwind Analysis: Pressure Contour

This case reinforced the suggestion that readings close to the radii on the top and side faces, in line as opposed to across the flow would be of more use to the project. These taps could be aligned to give results across the face in both headwind and backwind cases. Pressure gradients of regular, rectangular bodies such as that of the pallet, are well understood and are often calculated using the current method. Because of the similarity in gradient to the pallet, the rear face of the antenna was viewed as less of an area of interest, since a simple hand calculation would be sufficient. Subsequently, it was not seen as worthwhile to have a large number of pressure measurements from this face. The velocity plots for the backwind, shown Figure 7, demonstrate the movement in the wake of the radar. The wake appears much taller than that of the headwind case and a large vortex can be seen to form behind the radar.

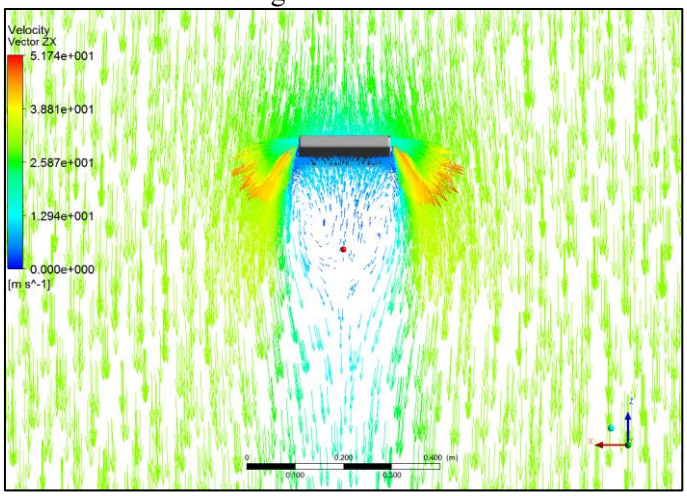

Figure 7 CFD Backwind Analysis: Velocity vector plots

3.4 Side-wind Case

Like the first two cases, the lowest pressure arose at the radial edges of the most buffeted surface in the flow stream. Again, the surfaces after this face are subjected to lower pressure but unlike previous cases this drops again when it reaches radii further downstream. This suggests that the air flow behaves in a different manner when presented with a face of greater length, as no such effect was seen for either the headwind or backwind case. Although no sizeable changes occur across the front or rear faces this area was highlighted as being of potential interest.

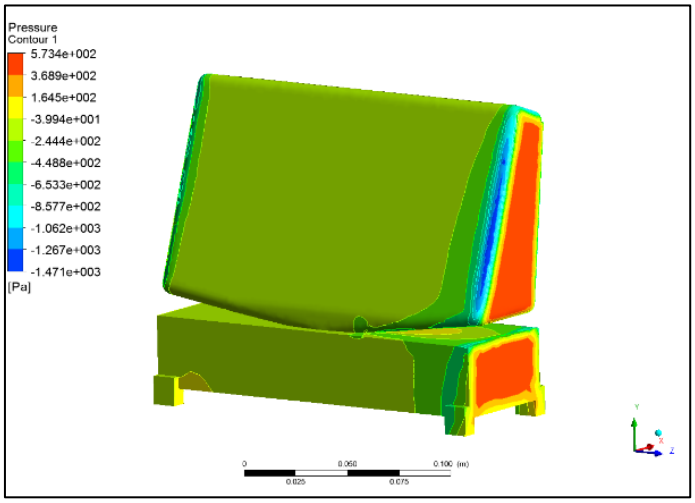

Figure 8 CFD Side Wind Analysis: Pressure Contour

It was in this case, that the underside face of the radar first warranted comment. An area of high pressure is produced between the antenna and the pallet, but this quickly reduces outwards in all directions to a comparatively low level. The gradient change was such that taps both along and across this face would display a measurable change.

For this case, with the wind direction at 90°, the side face was the face subject to the highest levels of pressure. This was displayed on Figure 9 as a peak in the centre of the face, where the flow of the air was most impeded. As the flow was forced outward, its velocity was increased, resulting in a subsequent decrease in pressure. The change follows an exponential relationship and can be seen at either side of the sample line.

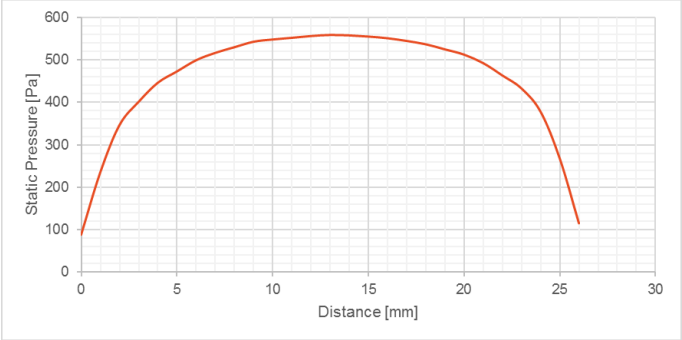

Figure 9 CFD Side Wind Analysis: Lateral gradient across side face

Figure 10 shows the velocity plots of the system. These demonstrate the difference in flow around the radar as a smaller cross-section is exposed to the wind; the wake created downwind of the body is far smaller than the preceding headwind and backwind cases.

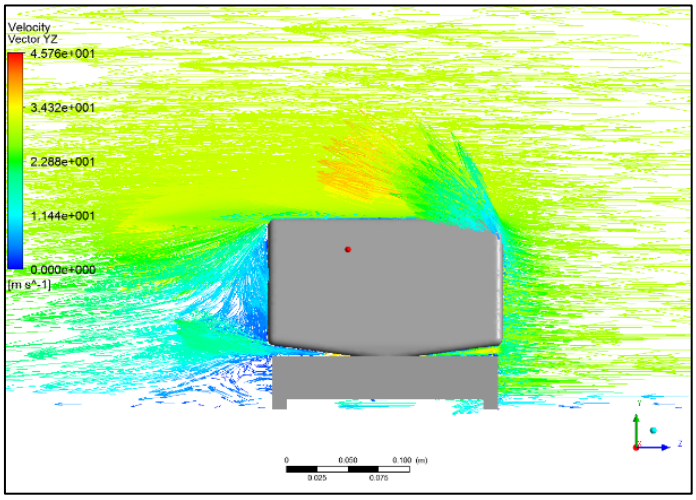

Figure 10 CFD Side Wind Analysis: Velocity vector plots

3.5 Angled-wind Case

The final case to be studied was when the wind was coming from a direction of 45° on to the front and side faces. Gradients along these two faces were similar although was somewhat accelerated on the side face, as indicated by the closer proximity of contours. The radius on the leading edge was subjected to the highest pressure and those at the points closest to the wall of the domain, were the lowest.

Suggested positioning for pressure readings deduced from the preceding cases, namely across the front and side faces, were also agreeable to this case.

The angled wind case was set up to analyse pressure gradients across the radar when faced with a wind coming from an angle of 45°. As shown on the contour plots, the leading surface was the radial edge between the side and the front faces. The sample lines were not altered for this case and so, in general are not aligned with the direction of the free stream flow.

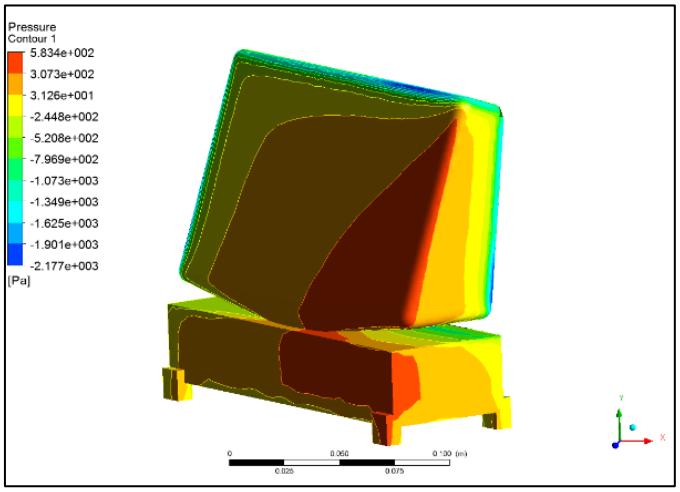

Figure 11 CFD Angled Wind Analysis: Pressure Contour

The velocity of the flow gradually increased as it moved across the surface of the radar before a more substantial rise in last 30mm of the front and 16mm of the side. The pressure reading near the trailing radial edge on the front face was lower than its counterpart on the side, indicating a later boundary layer separation on the shorter face.

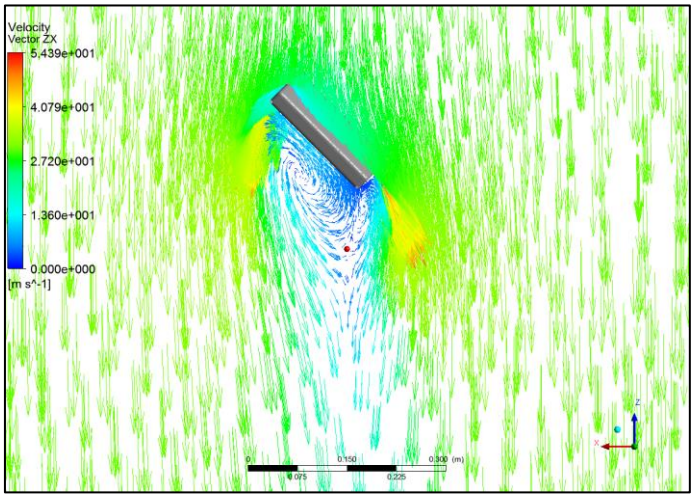

Figure 12 CFD Angled Wind Analysis: Velocity vector plots

The velocity plots, Figure 12, show the how the vortexes in the wake form and the behaviour of the flow as it moves around the radar.

4. measurements

4.1 Experimental Set Up

A 1:50 scale model was replicated and subjected to a wind tunnel test in the four case orientations. The scale model contained pressure taps at points that had been highlighted as of interest, from the CFD test case. The tunnel testing would provide a comparison to the CFD results and provide an indication of the validity of the computational analysis. The use of four orientations was beneficial as it gave a larger amount of data to analyse and any flow effects related to wind direction would be emphasized.

Like the domain in the CFD the model would ideally have a blockage ratio of <1% or 2% at a maximum. This would mean that the total surface area given by the model would be under 0.0327 or 0.0655 maximum. Using just the height and width calculations the scale of 1:50 had already been found to be suitable ($0.0296m^2$) as well as being manageable for the rapid prototyping machines.

To reduce cost and save time and complexity only the antenna structure would be 3D printed. In the SolidWorks software, the new model was created from the scaled dimensions and shelled to leave a hollow area inside. Pressure taps of 1mm were added to the model pre-print; although these would be too small for the pressure tubing, they allowed a reference point that could be bored out to the appropriate size. This was viewed a superior alternative to attempting to accurately drill holes on the model post print, where the risk of cracking or failure of the material would have been detrimental to the timescale of the project. Although initially all taps had been intended to occur on the centrelines of each face it was soon apparent that this could lead to interference between tubes on adjacent faces inside the model. Taps on the top and side faces were offset against each other by 2mm to avoid this problem. A hollow circular extrusion was added to interface with the pallet structure and provide a path for the tubing to run from inside the shell to the measuring equipment.

For the tubes to be easily accessible for any maintenance the model would be developed in two parts and bolted together. A useful feature in the SolidWorks software allowed the model to be developed as a single part and then split into two automatically created parts once the design for print was finalised. A rendering of the complete model and the split line of the is shown in **错误!未找到引用源。**. Another benefit of the model being developed in two halves was the decrease in time and cost. The job time of each side took approximately 17 hours, although two machines were utilised and were run simultaneously; a single piece would have taken much longer. Furthermore, the support material required for each job was drastically reduced.

Often shelled 3D printed models can often be difficult to produce; support material is required to fill the cavity and can be difficult to remove especially if fully enclosed. Relief holes are often added so that the material can drain out after sitting in the chemical bath. However, these are not always reliable leading to models leaking for sometimes days after completion.

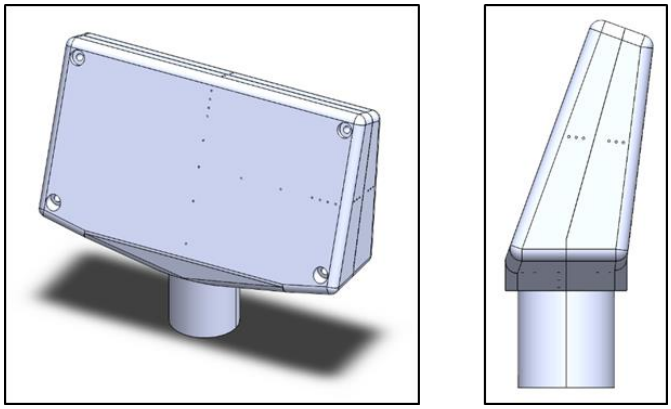

Figure 13 Print model of antenna (left) and split line creating two separate bodies (right)

Once printed the positional holes were drilled out to 1.8mm, wide enough for the metal tubing to fit in comfortably. The diameter of the hole was chosen to be as close to the diameter of the tubing as possible, so that results would not be affected by leakages. The metal tubing was cut using a Dremel multi-tool with a circular attachment into 10mm lengths; this accounted for the 4mm shell thickness and produced a protrusion of 6mm on which tubing could be attached using Araldite adhesive.

The pallet structure of the model, which served as a base for the antenna, was constructed using two parts of 18mm thick plywood. Two identical cross-sectional areas were drawn up and sawn out before being glued together with PVA. A hole of 40mm diameter was drilled into the pallet which would be where the 3D printed antenna would sit whilst allowing the tubing would be fed through the bottom of the tunnel and in to manometer. Small brackets where made from 4mm thick aluminium angle and screwed on to the side of the wooden block to give the require clearance of 6mm. The brackets would then interface with the floor of the wind tunnel.

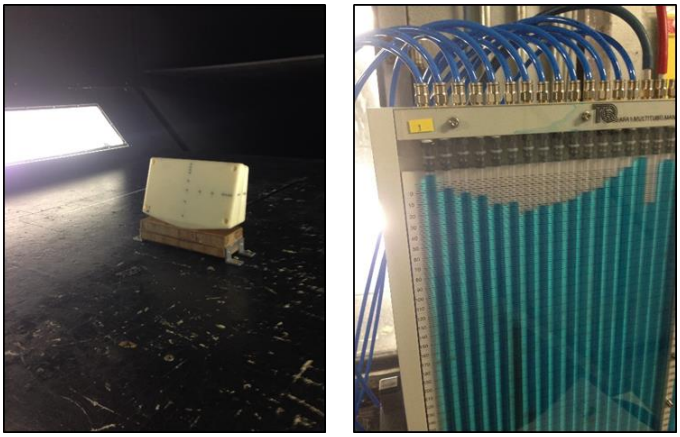

Figure 14 Model in wind tunnel for headwind case (left) and manometer displaying pressure readings during test run (right)

The air in the tunnel was accelerated to a velocity of 30m/s at which point the temperature and static pressure were recorded from the digital readout on the screen. The values from the manometer's 36 channels were taken and included a reading for free stream pressure and a readout not connected to a tube, which registered the pressure at atmosphere outside the tunnel. Each wind attack configuration was subjected to one test run and the results were recorded by hand once the determined velocity had been reached. These were later transferred into an excel spreadsheet where a pressure value for each tap could be analysed. Test runs were utilised to check for defective connections. Tap numbers 6, 13 and 15

were found to be either slow to react or altogether unresponsive. Following an investigation as to where a pinch may have occurred in the system each tapping was found to have a small blockage of glue impeding air flow. Using a small drill to free these blockages the model was re-tested, found to be satisfactory before experimental runs were proceeded with.

5. results

The experiment was designed to validate the CFD analysis, proving the method and set-up was suitable for use. Ideally, this would mean that data from the tunnel tests would be identical to the data from the computational analysis although, in practice, this rarely happens. However, through understanding the causes responsible for the differences in the two sets of data, improved designs and models can be made.

Using the same coordinates used to mark tap locations, pressure values were probed in the software so that results from the experiment could be directly compared. Figures were produced using both the CFD and recorded sets of data for each face and trend lines added to offer comparison. The x-axis is distance between each consecutive measurement location. For the headwind case, the CFD contour results had shown some interesting gradients across the front face of the antenna.

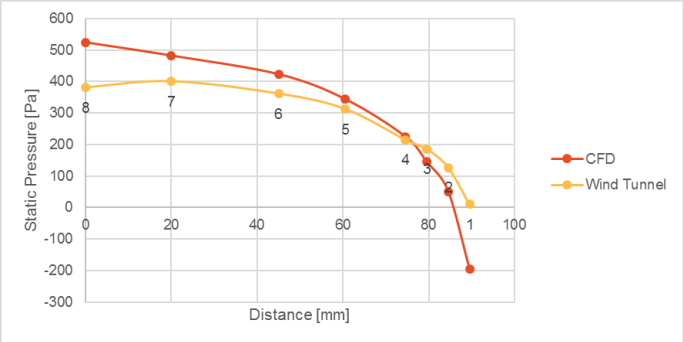

Figure 15 Headwind Experimental Analysis: Longitudinal gradient across the front face

The graph of the longitudinal taps on the face is shown in15. The data labels shown correspond to the tap numbers and are shown below the wind tunnel curve. Both sets of data indicated a decreasing trend as the wind moved up the face of the antenna. For the experimental data, the pressure drop off was not as steep when compared to the software solution. Although the both sets followed a curve the software predicted more extreme pressures in the highest and lowest laps. This is especially noticeable in the highest tap, where the software estimation is negative i.e. lower than atmospheric.

The point at which the results coincide, the intersection between the two curves, is between taps 3 and 4. These two taps were the third and fourth highest tap locations on the model, at 15mm and 20mm below the top frontal radius.

The taps on the underside of the radar had been expected to yield good results for the side and angled wind cases, although they produced some of the most valuable results for the headwind case. The experimental measurements, shown in Figure , displayed that the sudden decrease in pressure after a radius does occur, as predicted by the CFD. However, it this change initially occurred much quicker before the flow steadies. This seems to confirm the suggestion that a pressure increase does in fact occur on the top and side faces. This increase seems to happen much quicker and before the tap location closest to the radial edge.

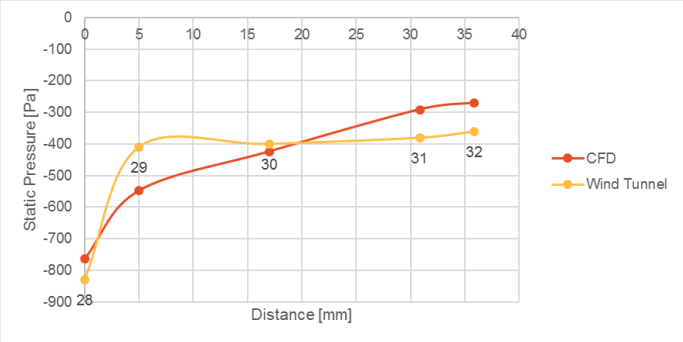

Figure 16 Headwind Experimental Analysis: Lateral gradient across the underside face

Finally, Figure 17 shows the linear trend for the pressure as the gap between antenna and pallet decreases. Both CFD and experiment display that the pressure increases as the passage for air to flow through, decreases. The average actual error for longitudinal trend was 38.7Pa and the average percentage error was 12.4%.

To summarise, the experiment confirmed broad observations of the CFD model, notably the surfaces of the antenna which are subjected to low pressure. The radial edges of the front face were identified, by the software, as being the areas with low-pressure readings. Though this could not be confirmed by the wind tunnel testing, it was evident that a substantial drop in pressure did occur across these features.

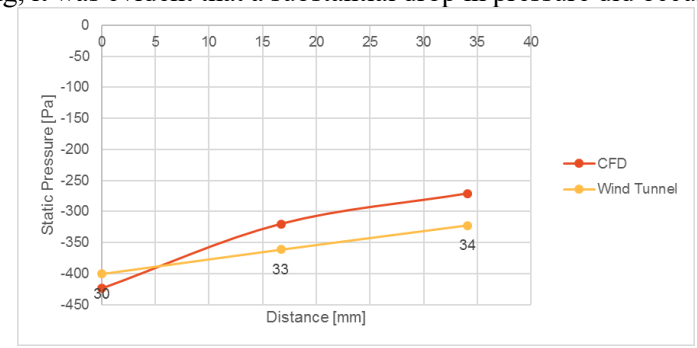

Figure 17 Headwind Experimental Analysis: Longitudinal gradient across the underside face

The front face of the radar was not subject to the magnitude of high pressure expected from the CFD model. Insufficient modelling of the boundary layer caused by the wind tunnel flooring may go some way as to explain this imbalance, which could have caused a lower stream velocity at the height of the antenna. Furthermore, the rate of pressure decrease across this face was not as severe in reality as on Fluent, although this may have been as a consequence of un-modelled test conditions, such as the surface roughness of the model. This could also have accounted for the gradients across faces in the wake being much steadier than those from the computational analysis, although this equally could have been caused by limitations of the k-ε model.

6. conclusions

The aim of the project was to investigate whether the current modelling of wind on an antenna for BAE systems could be improved upon using CFD. To undertake this study, an understanding of fluid dynamics and how they could be computed was required. CFD is a useful tool in engineering but for it to be confidently applied to the problem, its validity had to be confirmed. This, however, required that the approach taken in the set-up and usage of the Fluent software was assessed. These methodology studies sought to optimise and justify the actions of the project. They also provide good guidelines and practices that can be applied to further problems.

The results from the CFD analysis showed sensible characteristics and behaviours of the air around the radar which could be explained by theory. Analysis of gradients across the surfaces of the antenna demonstrated that the simple analytical method employed by the company was insufficient. The method ignored several aspects of the system which influenced the pressure distribution. The upwind radial

edges of the system were shown to have severe profiles across them with concentrations of very low pressure, as boundary layer separation occurred in these areas. The surfaces downwind, in the wake of the body, were subject to low pressure which would subject these faces to suction force. Taking account of these gradients would vastly improve the accuracy of any calculations and could be used to optimise antenna design.

To verify the findings of the CFD, a wind tunnel test was used, which also provided further insight into pressure distributions. Four orientations of wind direction were tested and measured readings were compared to CFD data. Each of the test cases had varying margins error; the headwind being the most accurately modelled with an average relative error of 33% between tested and computational results. Average relative errors for the backwind and side wind cases were 59% and 45% respectively. The high levels of error were likely to be caused by inadequate level of detail added to the set-up conditions of the CFD. A decision to assume that the faces of the model and wind tunnel behaved as non-slip surfaces was re-examined and found to be consequential to the results. Despite the inconsistency between the measured values and CFD solutions, the trends of the gradients which had been highlighted in the computational analysis could largely be seen to be present in the wind tunnel testing. From this, it can be concluded that CFD could be utilised to provide more accurate and in-depth pressure information than the simple theoretical method which is currently used by BAE Systems. However, the model which was developed over the course of this project requires more refinement. Additional improvements to the current Fluent set-up are recommended, which should be validated with further experimental testing before it can be successfully integrated into the radar design process. Reasonable deviation from theory is usually expected in experimental data, and, if sound reasoning can be given for any discrepancy, accepted. The CFD model had been modelled using many assumptions which could not be ignored in practice, namely the roughness of the tunnel floor surface. Furthermore, the manufacture of the model had ensured that any baseline assumptions on roughness were incorrect.

Should this experiment be repeated, some recommendations to improve the test integrity have been included. It is recommended to make the test model as large as possible (considering, of course, the blockage ratio and manufacturing limitations).

References

[1] Bailey, C. (2003) Guide to evaluating design wind loads to BS 6399-2: 1997. United Kingdom: Steel Construction Institute in Association with the Building Research Establishment and the British Constructional Steelwork Association.
[2] Bennett, G., Sherman, G. (1983), Analysis and thermal-design improvements of downhole tools for use in hot-dry wells http://www.osti.gov/pages/190 servlets/purl/6491119, doi:10.2172/6491119,.
[3] Buresti, G. (2000) Bluff-Body Aerodynamics. [online]. Available from: https://www.mech.kth.se/courses/5C1211/BluffBodies.pdf [Accessed 6 March 2017].
[4] Harper, J., Pope, A. & Rae, W. (1984) Low-speed wind tunnel testing. 2nd edition. New York: John Wiley & Sons.
[5] Holmes, J. (2007) Wind loading of structures. 1st edition. London [u.a.]: Taylor & Francis.
[6] Knapp, G. (2007) Improved Methods for Structural Wind Engineering.
[7] MacDonald, A. (1975) Wind loading on buildings. 1st edition. London: Applied science publishers.
[8] Murakami, S. (1998) Overview of turbulence models applied in CWE–1997. Journal of Wind Engineering and Industrial Aerodynamics. 74-76pp. 1-24.
[9] Qin, N. & Harris, M. (2013) Flow Feature Aligned Mesh Generation and Adaptation
[10] Reiter, S. (2008) Validation Process for CFD Simulations of Wind Around Buildings. [online]. Available
[11] from: https://www.researchgate.net/profile/Sigrid_Reiter/publication/267299689_Validation_Process_for_CFD_Simulations_of_Wind_Around_Buildings/links/5475963c0cf2778985aee212.pdf.
[12] Scanlon, T., Taylor, I., Bicanic, N., Lim, J. & Clannachan, G. (2009) Practical application of CFD for wind loading on tall buildings. Proceedings of the 7th International Conference on Tall Buildings.

[13] Xu, S., Li, Q. & Huang, S. (2007) Numerical evaluation of wind effects on a tall steel building by CFD [online]. Journal of Constructional Steel Research. 63 (5), pp. 612–627.